Journal of Geophysical Research: Earth Surface

Supporting Information for

Controls on Larsen C Ice Shelf retreat from a 60-year satellite data record

Shujie Wang[1,2,3], Hongxing Liu[4,5], Kenneth Jezek[6], Richard B. Alley[2,7], Lei Wang[8], Patrick Alexander[9], and Yan Huang[5]

[1]Department of Geography, Pennsylvania State University, University Park, PA 16802, USA.

[2]Earth and Environmental Systems Institute, Pennsylvania State University, University Park, PA 16802, USA.

[3]Institute for Computational and Data Sciences, Pennsylvania State University, University Park, PA 16802, USA.

[4]Department of Geography, University of Alabama, Tuscaloosa, AL 35487, USA.

[5]Key Laboratory of Geographic Information Science, Ministry of Education, East China Normal University, Shanghai 200241, China.

[6]School of Earth Sciences, Ohio State University, Columbus, OH 43210, USA.

[7]Department of Geosciences, Pennsylvania State University, University Park, PA 16802, USA.

[8]Department of Geography & Anthropology, Louisiana State University, Baton Rouge, LA 70803, USA.

[9]Lamont-Doherty Earth Observatory, Columbia University, Palisades, NY 10964, USA.

Contents of this file

Introduction

This supporting document includes more details about the preprocessing of satellite imagery (Text S1) and ice shelf modeling (Text S2), one supplementary figure (Figure S1), and one table (Table S1). Figure S1 shows the time series of Larsen C front locations from 1963 to 2020. Table S1 provides detailed information on the image sources, time periods, and estimated accuracies for flow velocity derivation over multiple periods.

Text S1. Satellite images and preprocessing

The images we used for this study include declassified intelligence satellite photographs (DISP) acquired by the ARGON mission, optical images acquired by the Landsat-4/5 TM, Landsat-7 ETM+, and Landsat-8 OLI sensors, and synthetic aperture radar (SAR) images acquired by the ERS-1, ERS-2, Radarsat-1, Envisat, and ALOS satellites.

The DISP images were acquired by the ARGON KH-5 panchromatic camera from an orbital altitude of 322 km at a ground resolution of 140 m. Trackable features such as crevasses, rifts, and flow bands are visible on the images. We orthorectified the DISP images using a rigorous camera model with bundle block adjustment based on a set of ground control points (GCPs) selected from very high-resolution WorldView images (Wang et al., 2016). The Landsat images were provided as L1G or L1GT products via the USGS EarthExplorer data portal, and were georeferenced and orthorectified by the USGS EROS data center. The Radarsat-1 images were orthorectified and mosaiced by the Byrd Polar and Climate Research Center for the Radarsat Antarctic Mapping Project (RAMP) (Jezek et al., 1998; Jezek, 2003). The ALOS PALSAR images were accessed from the Alaska Satellite Facility data portal, and were geocoded and orthorectified by the Japan Aerospace Exploration Agency. The ERS-1, ERS-2, and Envisat SAR images were provided by the European Space Agency. We geocoded and orthorectified these SAR images using the PRARE precise orbit data for ERS-1/2 and the DORIS precise orbit data for Envisat in the ENVI® SARscape® software. The RAMP digital elevation model 2 (Liu et al., 2001) was used for image orthorectification. The accuracy of geolocation using the precise orbit data is estimated to be better than one pixel (Small et al., 2007). The speckle noise of SAR imagery was suppressed by applying gamma and median filters. For images used for velocity derivation, we also conducted image-to-image co-registration for each image pair to ensure the relative error of image alignment is less than one pixel. To enhance the surface features on imagery for velocity mapping, we divided each image pair into multiple segment pairs and performed image histogram stretching.

Text S2. Ice shelf modeling experiments

We used the Ice-sheet and Sea-level System Model (ISSM), developed by the Jet Propulsion Laboratory and the University of California at Irvine (Larour et al., 2012), to conduct the ice shelf modeling experiments. We used the shallow shelf approximation (SSA) model (MacAyeal 1989; Weis et al. 1999; Morland 1987) to examine how ice shelf flow velocities and stress conditions vary with front retreat and rift development. The SSA model assumes a hydrostatic equilibrium condition and depth-invariant horizontal velocity, described as:

$$\frac{\partial}{\partial x}\left(2\eta h(2\frac{\partial u}{\partial x}+\frac{\partial v}{\partial y})\right)+\frac{\partial}{\partial y}\left(\eta h(\frac{\partial u}{\partial y}+\frac{\partial v}{\partial x})\right)=\rho g h\frac{\partial s}{\partial x} \quad (1)$$

$$\frac{\partial}{\partial y}\left(2\eta h(2\frac{\partial v}{\partial y}+\frac{\partial u}{\partial x})\right)+\frac{\partial}{\partial x}\left(\eta h(\frac{\partial u}{\partial y}+\frac{\partial v}{\partial x})\right)=\rho g h\frac{\partial s}{\partial y} \quad (2)$$

where x and y are horizontal cartesian coordinates, u and v are the velocity components in the x and y directions, g is the gravitational acceleration (9.81 m/s^2), h is the ice thickness, s is the surface elevation, ρ is the ice density (916 kg/m^3), and η is the effective viscosity given by:

$$\eta=\frac{1}{2}\bar{B}[(\frac{\partial u}{\partial x})^2+(\frac{\partial v}{\partial y})^2+\frac{\partial u}{\partial x}\frac{\partial v}{\partial y}+\frac{1}{4}(\frac{\partial u}{\partial y}+\frac{\partial v}{\partial x})^2]^{(1-n)/2n} \quad (3)$$

where $\bar{B}$ is the vertically averaged hardness and represents the ice rigidity, and *n* is Glen's flow law exponent.

ISSM is based on a finite element numerical modeling scheme. The ice rigidity parameter $\bar{B}$ can be solved for through inversion by minimizing the differences between modeled and observed flow velocities. For model configuration, we used the anisotropic mesh adaptation method to generate the numerical mesh net nodes. The surface elevations were obtained from the Antarctic digital elevation model created from ERS-1 radar and ICESat laser altimetry data (Bamber et al., 2009). The ice shelf thickness *(h*) was calculated based on the hydrostatic equilibrium condition:

$$h=\left(\frac{\rho'}{\rho'-\rho}\right)\times s \quad (4)$$

where ρ' is the seawater density (1028 kg/m^3), *s* is the surface elevation, and ρ is the ice density (916 kg/m^3).

Using the modeled flow velocity field and parameter $\bar{B}$, we calculated the deviatoric stresses, including longitudinal deviatoric stresses, first principal stresses, and second principal stresses. The deviatoric stress (τ) is calculated as:

$$\tau=2\eta\dot{\epsilon} \quad (5)$$

where η is the effective viscosity (equation 3), and $\dot{\epsilon}$ is the corresponding strain rate. In a horizontal Cartesian system, the strain rates ($\dot{\epsilon}_x, \dot{\epsilon}_y, \dot{\epsilon}_{xy}$) are calculated as:

$$\dot{\epsilon}_x = \frac{\partial u}{\partial x} \tag{6}$$

$$\dot{\epsilon}_y = \frac{\partial v}{\partial y} \tag{7}$$

$$\dot{\epsilon}_{xy} = \frac{1}{2}\left(\frac{\partial u}{\partial y} + \frac{\partial v}{\partial x}\right) \tag{8}$$

Following Alley et al. (2018), the longitudinal strain rate ($\dot{\epsilon}_{lon}$, along the flow direction) can be calculated as:

$$\dot{\epsilon}_{lon} = \dot{\epsilon}_x \cos^2\alpha + 2\dot{\epsilon}_{xy}\cos\alpha\sin\alpha + \dot{\epsilon}_y \sin^2\alpha \tag{9}$$

where α is the flow angle that is counter-clockwise from the *x* axis.

The magnitudes of the maximum ($\dot{\epsilon}_{first}$, first principal) and minimum ($\dot{\epsilon}_{second}$, second principal) tensile principal strain rates can be calculated as:

$$\dot{\epsilon}_{first} = \frac{1}{2}\left(\dot{\epsilon}_x + \dot{\epsilon}_y\right) + \sqrt{\frac{1}{4}\left(\dot{\epsilon}_x - \dot{\epsilon}_y\right)^2 + \dot{\epsilon}_{xy}{}^2} \tag{10}$$

$$\dot{\epsilon}_{second} = \frac{1}{2}\left(\dot{\epsilon}_x + \dot{\epsilon}_y\right) - \sqrt{\frac{1}{4}\left(\dot{\epsilon}_x - \dot{\epsilon}_y\right)^2 + \dot{\epsilon}_{xy}{}^2} \tag{11}$$

$$\theta = \frac{1}{2}\left[arctan\left(\frac{2\dot{\epsilon}_{xy}}{\dot{\epsilon}_x - \dot{\epsilon}_y}\right)\right] \tag{12}$$

where θ is the angle between the y axis and the first principal axis if $\dot{\epsilon}_x < \dot{\epsilon}_y$, or between the y axis and the second principal axis if $\dot{\epsilon}_x > \dot{\epsilon}_y$.

Following Cuffey and Paterson (2010), the backstress (σ_b) can be calculated as

$$\sigma_b = \frac{1}{2}\rho g\left(1 - \frac{\rho}{\rho'}\right)h - 2\eta(2\dot{\epsilon}_x + \dot{\epsilon}_y) \tag{13}$$

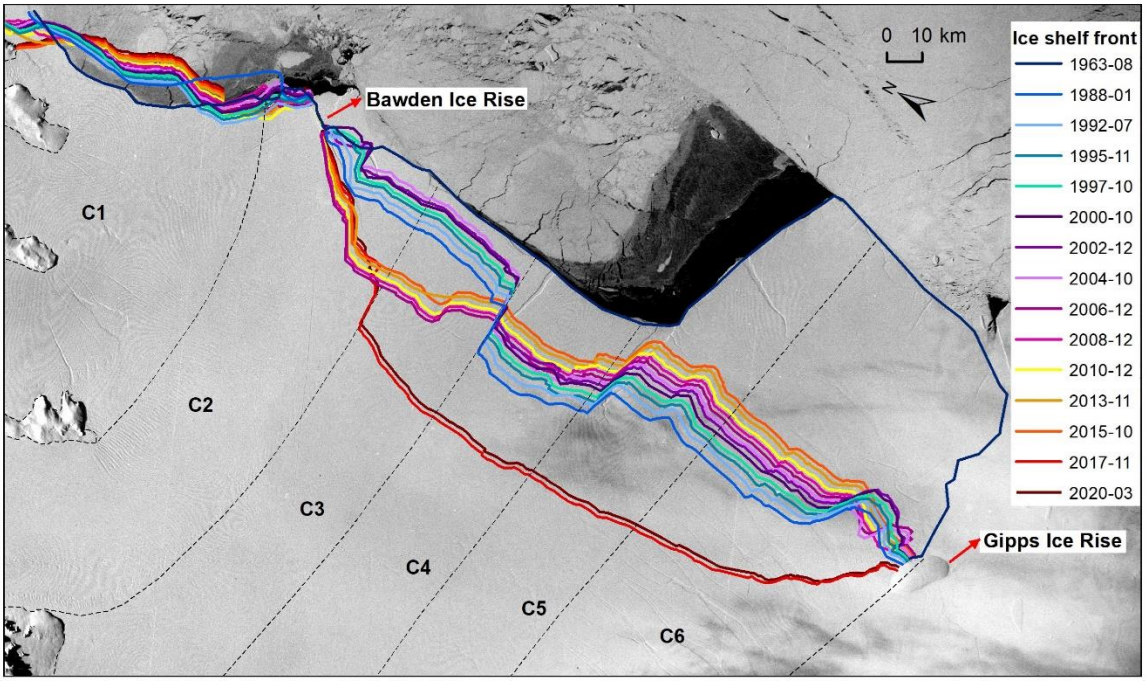

Figure S1. Ice front locations of Larsen C from 1963 to 2020. The background image is the georeferenced DISP image acquired in 1963.

Period	Image source	Displacement uncertainty (m)	Time separation (years)	Velocity uncertainty (m/year)
1963/08–1988/01	DISP, Landsat TM	90	24.4	3.7
1986/03–1988/01	Landsat TM	45	1.8	25
1997/10–2000/09	Radarsat SAR	37.5	3.0	12.5
2000/01–2002/12	Landsat ETM+	22.5	1.9	11.8
2006/06–2008/10	ALOS PALSAR	22.5	2.4	9.4
2008/10–2010/10	ALOS PALSAR	22.5	2.0	11.3
2013/11–2015/11	Landsat OLI	22.5	2.0	11.3
2015/11–2016/12	Landsat OLI	22.5	1.1	20.5
2016/12–2017/12	Landsat OLI	22.5	1.0	22.5
2017/12–2019/02	Landsat OLI	22.5	1.3	17.3
2019/02–2020/03	Landsat OLI	22.5	1.1	20.5

Table S1. Image sources, time periods, and estimated uncertainties for ice velocity derivation.